ORGANOMETALLICS

Article

pubs.acs.org/Organometallics

Synthesis and Reactivity of Sterically Encumbered Diazaferrocenes

Markus Kreye, Dirk Baabe, Peter Schweyen, Matthias Freytag, Constantin G. Daniliuc,† Peter G. Jones, and Marc D. Walter*

Institut für Anorganische und Analytische Chemie, Technische Universität Braunschweig, Hagenring 30, 38106 Braunschweig, Germany

Supporting Information

ABSTRACT: Bulky pyrrolyl ligands have been used for the synthesis of diazaferrocenes, which have been characterized by various spectroscopic techniques, including X-ray diffraction for *rac*-[{η^5-2,3,5-$(Me_3C)_3C_4HN$}$_2$Fe]. Chemical oxidation of diazaferrocenes to the corresponding diazaferrocenium cations has been accomplished with $AgSbF_6$. In addition, EPR and Mössbauer spectroscopic, electrochemical, and density function theory (DFT) studies have provided a more detailed understanding of the electronic structures of these complexes.

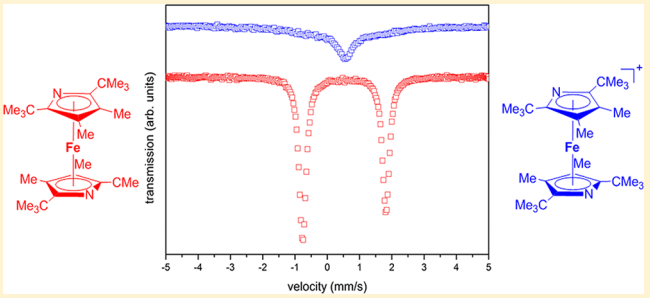

INTRODUCTION

With the landmark discovery of ferrocene, [(η^5-C_5H_5)$_2$Fe],[1] cyclopentadienyls became one of the most widely used ancillary ligands in organometallic chemistry.[2] Their low intrinsic reactivity combined with easily modified steric and electronic properties make them excellent spectator ligands in various applications, including polymerization and small-molecule activation.[3] Furthermore, ferrocene-derived ligands have become indispensable in catalysis.[4]

In contrast, heterocyclic derivatives such as C_4H_4E (E = N, P, As, Sb), in which a CH group of C_5H_5 has been replaced by an iso(valence)-electronic and isolobal group 15 element, have not been extensively investigated.[5] A pitfall in this series is provided by the nitrogen-based pyrrolyl system. Whereas iron and manganese complexes with one pyrrolyl ligand were prepared shortly after the discovery of ferrocene,[6] diazaferrocene, [(η^5-C_4H_4N)$_2$Fe], remains elusive and only ill-defined products were obtained from the reaction of $FeCl_2$ with 2 equiv of $(C_4H_4N)Li$[7] or $(C_4H_4N)Na$.[8] The instability of [(η^5-C_4H_4N)$_2$Fe] was attributed to η^5–κ^1 haptotropic shifts of the pyrrolyl ligand.[6c,9] An interesting observation in this context is the reaction of *meso*-disubstituted pyrrole with [Fe{N(SiMe$_3$)$_2$}$_2$(thf)] to form a tetranuclear iron cluster, which combines two η^5-diazaferrocene units and two iron centers with a distorted tetrahedral κN coordination.[10] Because of the problems encountered with diazaferrocene, research efforts have mainly focused on azaferrocenes and the synthesis of moderately substituted derivatives such as [(η^5-C_5Me_5)Fe(η^5-C_4H_4N)] and [(η^5-C_5H_5)$_2$Fe(η^5-2,5-$Me_2C_4H_2N$)].[6c,11] In the early 1990s Kuhn introduced several sterically encumbered pyrrolyls, which stabilize η^5 coordination by effectively blocking the κN coordination mode.[5,12] With tetramethylpyrrolyl the formation of a thermally unstable [(κ^1-C_4Me_4N)$_2$Fe(thf)$_2$] complex was reported,[13] which decomposed in solution. However, in the presence of small quantities of water the structurally characterized tetramethylpyrrole adduct of octamethyldiazaferrocene, [(η^5-C_4Me_4N)$_2$Fe](C_4Me_4NH)$_2$, was isolated. The stability of [(η^5-C_4Me_4N)$_2$Fe] was attributed to hydrogen bond formation between the N atoms of the diazaferrocene fragment and the free tetramethylpyrroles, which reduces the charge density at the N atoms.[7b] Increasing the steric demand at the 2,5-positions of the pyrrolyl provided sufficient steric protection to isolate and structurally characterize [(η^5-Pyr^{tBu_2})$_2$Fe] (Pyr^{tBu_2} = 2,5-$(Me_3C)_2C_4H_2N$, **1-Fe**).[5,14] Subsequently, pyrrolyl **1** has also been used for the synthesis of other transition-,[15] rare-earth-,[16] and main-group-metal complexes.[17] However, the majority of these investigations were undertaken in the early 1990s and since then sterically demanding pyrrolyl ligands have been only sporadically studied.[12,15–17] Our first contributions to this area consisted in the preparation of various azatrozircene complexes, [(η^7-C_7H_7)Zr(η^5-Pyr′)],[18] starting from the pyrrolyl anions **1**, **3**, and **5** (Figure 1) and [(η^7-C_7H_7)ZrCl(tmeda)].[19] The [(η^7-C_7H_7)Zr]$^+$ fragment can coordinate various monoanionic ligands[19,20] and serves as an ideal platform for cone angle measurements.[19,20d]

In this contribution, we extend our study to iron and report on the synthesis of a series of novel sterically demanding diazaferrocenes and their structures and electronic properties. We also compare these results to those of their ferrocene analogues.

RESULTS AND DISCUSSION

Synthesis and Characterization of Diazaferrocenes. Sterically encumbered cyclopentadienyl ligands[2a] have success-

Special Issue: Ferrocene - Beauty and Function

Received: May 27, 2013
Published: July 29, 2013

   dx.doi.org/10.1021/om400474e | Organometallics 2013, 32, 5887–5898

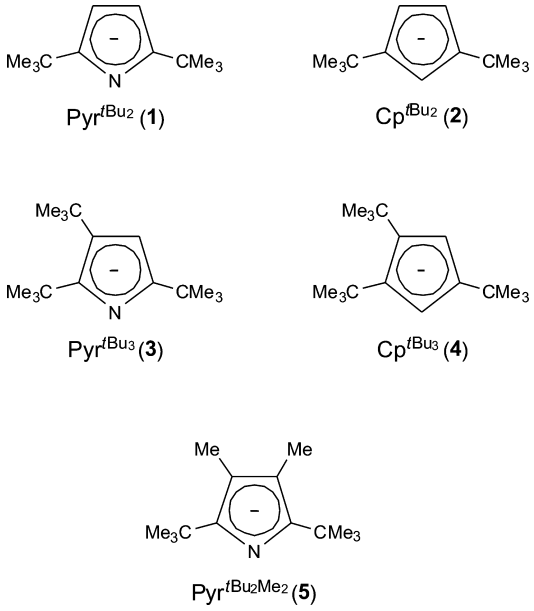

Figure 1. Bulky (hetero)cyclic π ligands discussed in this paper.

fully been used to stabilize manganese(II)[21] and iron(II)[22] half-sandwich complexes kinetically with respect to the thermodynamically favored metallocene formation. For example, 1,2,4-tri-*tert*-butylcyclopentadienyl (**4**) allows the isolation of the iron half-sandwich complex $[\{\eta^5\text{-}1,2,4\text{-}(Me_3C)_3C_5H_2\}FeI]_2$ (**4-FeI**) (Scheme 1).[22g] Whereas **1** and **2** are not sterically demanding enough to stabilize a half-sandwich species, 2,3,5-tri-*tert*-butylpyrrolyl (**3**) has steric properties similar to those of its carbocyclic counterpart (**4**).[19] We therefore decided to explore the potential of **3** in the synthesis and stabilization of iron half-sandwich derivatives. Pyrrolide **3-K** reacts with $FeI_2(thf)_2$ in THF to form a deep red solution. Although suitable trapping experiments on this solution suggested the presence of the desired iron half-sandwich complex,[23] only the purple $[\{\eta^5\text{-}2,3,5\text{-}(Me_3C)_3C_4HN\}_2Fe]$ (**3-Fe**) was isolated when we attempted to isolate the half-sandwich intermediate **3-FeI**. The reduced stability of **3-FeI** is most probably a kinetic effect. The iron atoms in **4-FeI** adopt a high-spin (S = 2) configuration, which results in rather long and weak Fe−C bonds;[22g] therefore, η^5-κ^1 haptotropic shifts are probably relatively facile in **3-FeI**. Furthermore, diazaferrocene formation provides a strong thermodynamic driving force.

The diazaferrocene **3-Fe** is thermally very stable and—like its ferrocene counterpart **4-Fe**—very soluble in all common organic solvents. However, single crystals of **3-Fe** may be grown from saturated hexamethyldisiloxane solutions at −30 °C. Diazaferrocene **3-Fe** and ferrocene **4-Fe** crystallize with approximate (noncrystallographic) C_2 symmetry (Table 1).[22g] Figure 2 shows the molecular structure of **3-Fe**, and selected bond angles and distances of **3-Fe** and **4-Fe** are collected in Table 2. As expected, no significant structural changes are induced when a CH group is replaced by an N atom.

Despite the very similar solid-state structures of **3-Fe** and **4-Fe**, the NMR spectra of **3-Fe** are peculiar. Six broad and partially overlapping *t*Bu resonances are observed in the ^{1}H NMR spectrum, which can be divided into two sets. The 2,3,5-tri-*tert*-butylpyrrolyl ligand (**3**) can form different isomers, varying only in the face to which the metal is coordinated. Depending on the face bound to the metal, the pyrrolyl group can be right-handed or left-handed. Therefore, four isomers need to be considered, which can be divided into two pairs of mirror images of C_2 (*rac*) or C_s (*meso*) symmetry, respectively (Scheme 2). The two optically active species (C_2) are indistinguishable energetically and magnetically, but they can be differentiated from the *meso* isomer.

However, NMR spectroscopy provides no evidence for the presence of the *meso* isomer or a paramagnetic κ^1N-bound

Scheme 1

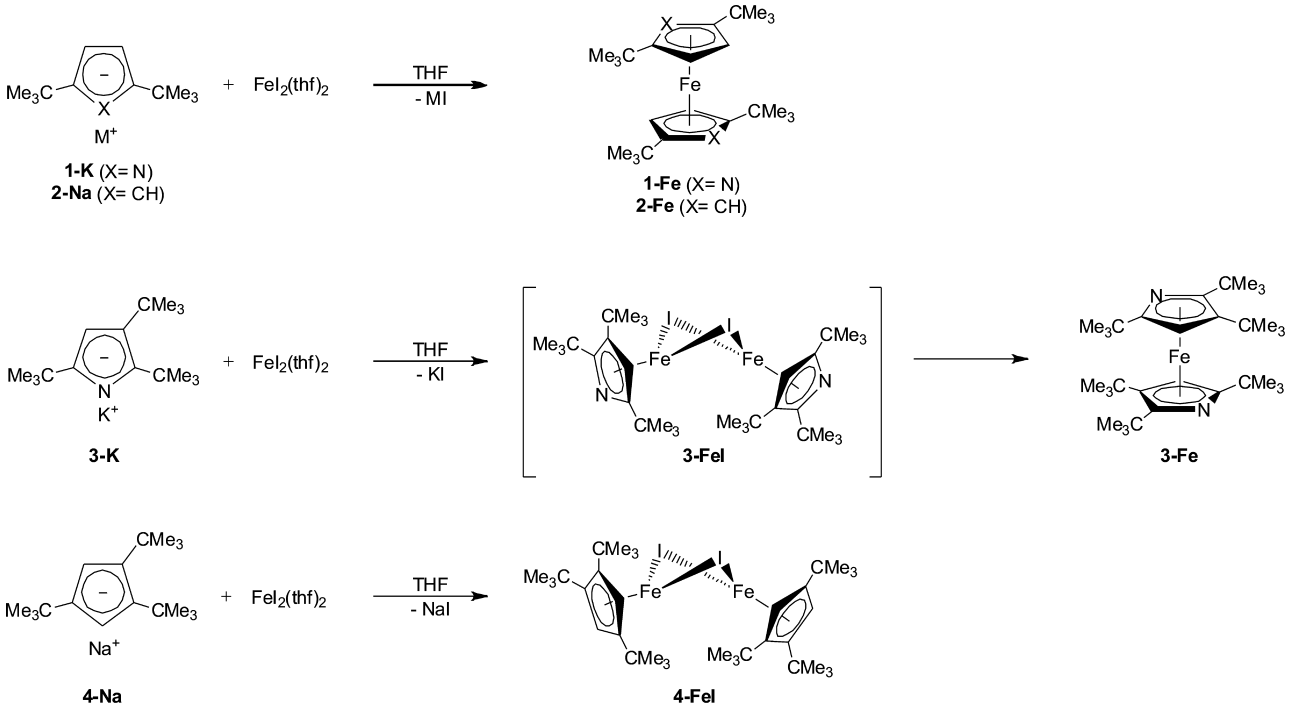

dx.doi.org/10.1021/om400474e | *Organometallics* 2013, 32, 5887−5898

Table 1. Crystallographic Data

	3-Fe	[4-Fe][SbF_6]	[5-Fe][SbF_6]·CH_2Cl_2
empirical formula	$C_{32}H_{56}FeN_2$	$C_{34}H_{58}F_6FeSb$	$C_{29}H_{50}Cl_2F_6FeN_2Sb$
formula wt	524.64	758.40	789.21
temp (K)	100(2)	100(2)	100(2)
wavelength λ (Å)	1.54184	1.54184	0.71073
cryst syst	orthorhombic	monoclinic	triclinic
space group	$Pna2_1$	$C2/c$	$P\bar{1}$
a (Å)	16.9680(2)	19.6586(10)	10.5350(4)
b (Å)	20.8368(2)	14.7578(8)	12.3074(5)
c (Å)	17.5847(2)	12.1964(8)	14.1764(6)
α (deg)	90	90	78.320(2)
β (deg)	90	104.070(6)	76.264(2)
γ (deg)	90	90	77.315(2)
V (Å^3)	6217.23(12)	3432.2(3)	1719.90(12)
Z	8	4	2
no. of rflns collected	101249	31772	87055
no. of indep rflns (R_{int})	11776 (0.0446)	3584 (0.0852)	10217 (0.0557)
goodness of fit on F^2	1.031	1.044	1.069
ρ_{calcd} (g cm^{-3})	1.121	1.468	1.524
μ (mm^{-1})	4.022	10.091	1.416
$R(F_o)$ ($I > 2\sigma(I)$)	0.0288	0.0319	0.0301
$R_w(F_o^2)$	0.0724	0.0753	0.0603
$\Delta\rho$ (e Å^{-3})	0.216/−0.283	0.377/−0.946	0.968/−0.935

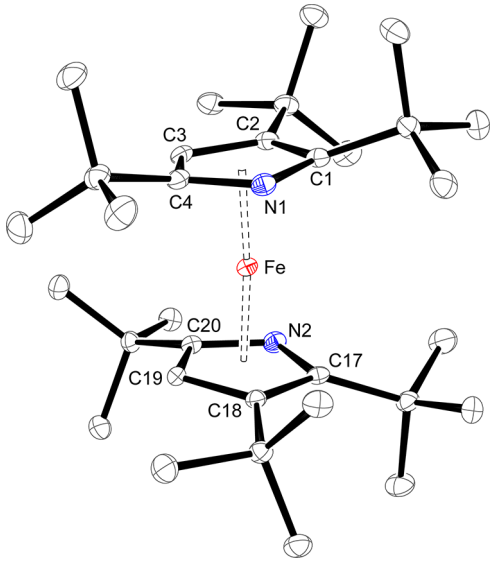

Figure 2. ORTEP diagram of **3-Fe** with thermal displacement parameters drawn at the 50% probability level. Only one of the two independent molecules in the asymmetric unit is shown for **3-Fe**. The average displacement of quaternary CMe_3 carbons on C1, C4, C17, and C20 from the ring plane is 0.44 Å.

species, but the NMR data are consistent with two C_2-symmetric isomers, which are not equally populated. Both isomers exchange at ambient temperature on the NMR time scale, as shown by an ^{1}H−^{1}H NOESY experiment (Figure 3), which suggests that they are rotamers.

From the ratio of the two isomers (1.73:1 at 28 °C) a slight thermodynamic preference, $\Delta G(301\ K) = -RT \ln K_{eq} = -0.33$ kcal mol^{-1}, for one isomer can be calculated. The variable-temperature (VT) NMR spectra of **3-Fe** recorded between 28 and 93 °C are shown in the Supporting Information. For the slow-exchange regime a barrier of $\Delta G^{\ddagger}$ = 17.5 kcal mol^{-1} (38 °C) is calculated from the line shapes,[24] whereas a lower barrier of $\Delta G^{\ddagger}$ = 14.2 kcal mol^{-1} was determined for the carbocyclic analogue **4-Fe**.[22g] For **1-Fe** and **2-Fe**, the reverse trend of $\Delta G^{\ddagger}$ = 9.9 and 13.2 kcal mol^{-1}, respectively, is noteworthy.[15d] The lower rotational barrier for **1-Fe** has been rationalized on the basis of extended Hückel and MNDO calculations, by a weaker iron−ring bond, more favorable ring slippage in the direction of the N atom, and a greater flexibility of the *ipso*-C bond, which allows the *t*Bu group of the pyrrolyl ligand to bend out of the ring plane more easily than in the cyclopentadienyl system.[15c] However, He I photoelectron studies on **1-Fe** and **2-Fe** contradict the first argument, since the Fe−Pyr bond is thermodynamically more stable than the Fe−Cp bond.[9c] This and the fact that the additional *t*Bu groups in the 3,3′-positions of **3-Fe** make ring slippage and tilting of the pyrrolyl rings less favorable may explain the increased rotational barrier for **3-Fe** relative to **1-Fe** and **4-Fe**.

The steric demand of the tetrasubstituted pyrrolyl **5** is intermediate between those of **1** and **3**;[19] no half-sandwich intermediate was detected, and the diazaferrocene **5-Fe** was readily isolated (Scheme 3). The connectivity in **5-Fe** can be confirmed by X-ray crystallography, but the molecular structure could not be determined with high accuracy because of unexpectedly large residual electron density in proximity to the iron atom, which could not be modeled satisfactorily. Despite several attempts to grow higher quality crystals under various

Table 2. Structural Comparison between 3-Fe and 4-Fe

param[a]	3-Fe	4-Fe[22g]	4-Fe$^+$
Fe/Fe′−N1/N1′,[b] Å	2.0722(15)/ 2.0717(16)	2.077(2)/ 2.056(2)	2.113(2)
Fe/Fe′−C1/C1′, Å	2.1197(18)/ 2.1111(18)	2.110(2)/ 2.115(2)	2.201(2)
Fe/Fe′−C2/C2′, Å	2.1213(18)/ 2.1458(18)	2.060(2)/ 2.075(2)	2.180(2)
Fe/Fe′−C3/C3′, Å	2.0665(17)/ 2.0778(18)	2.119(2)/ 2.127(2)	2.100(2)
Fe/Fe′−C4/C4′, Å	2.0748(17)/ 2.0731(19)	2.139(2)/ 2.115(2)	2.154(2)
Fe/Fe′−N2/N2′,[b] Å	2.0736(14)/ 2.0665(16)	2.059(2)/ 2.079(2)	2.113(2)
Fe/Fe′−C17/C17′, Å	2.1222(17)/ 2.1100(19)	2.109(2)/ 2.103(2)	2.201(2)
Fe/Fe′−C18/C18′, Å	2.1256(17)/ 2.1288(18)	2.075(2)/ 2.063(2)	2.180(2)
Fe/Fe′−C19/C19′, Å	2.0537(18)/ 2.0620(17)	2.132(2)/ 2.122(2)	2.100(2)
Fe/Fe′−C20/C20′, Å	2.0615(18)/ 2.0579(18)	2.114(2)/ 2.158(2)	2.154(2)
Fe−ring (av), Å	2.09(3)	2.10(3)	2.15(4)
Δ,[c] Å	0.01		0.04
Pyr/Cp_{cent}−Fe (av), Å	1.710	1.713	1.771
Pyr/Cp_{plane}−Fe (av), Å	1.709	1.713	1.770
Pyr/Cp_{cent}−Fe−Pyr/ Cp_{cent}, deg	175	175	175
interplanar angle between rings, deg	8.13/7.87	7.77/7.12	8.71

[a] A prime (′) denotes the second independent molecule of **3-Fe** or **4-Fe** in the asymmetric units. [b] For a Cp ligand this is the distance between the iron and a C−H group. [c] Ring slippage in the direction of the N atom as defined by Δ = 0.5[(Fe−C3/18) + (Fe−C4/19)] − 0.5[(Fe−C2/17) + (Fe−C4/20)].

dx.doi.org/10.1021/om400474e | *Organometallics* 2013, 32, 5887−5898

Scheme 2

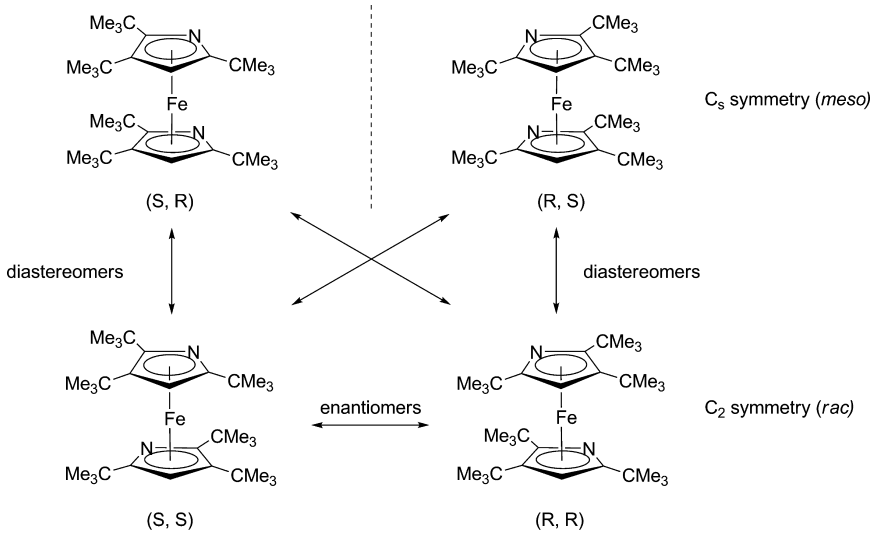

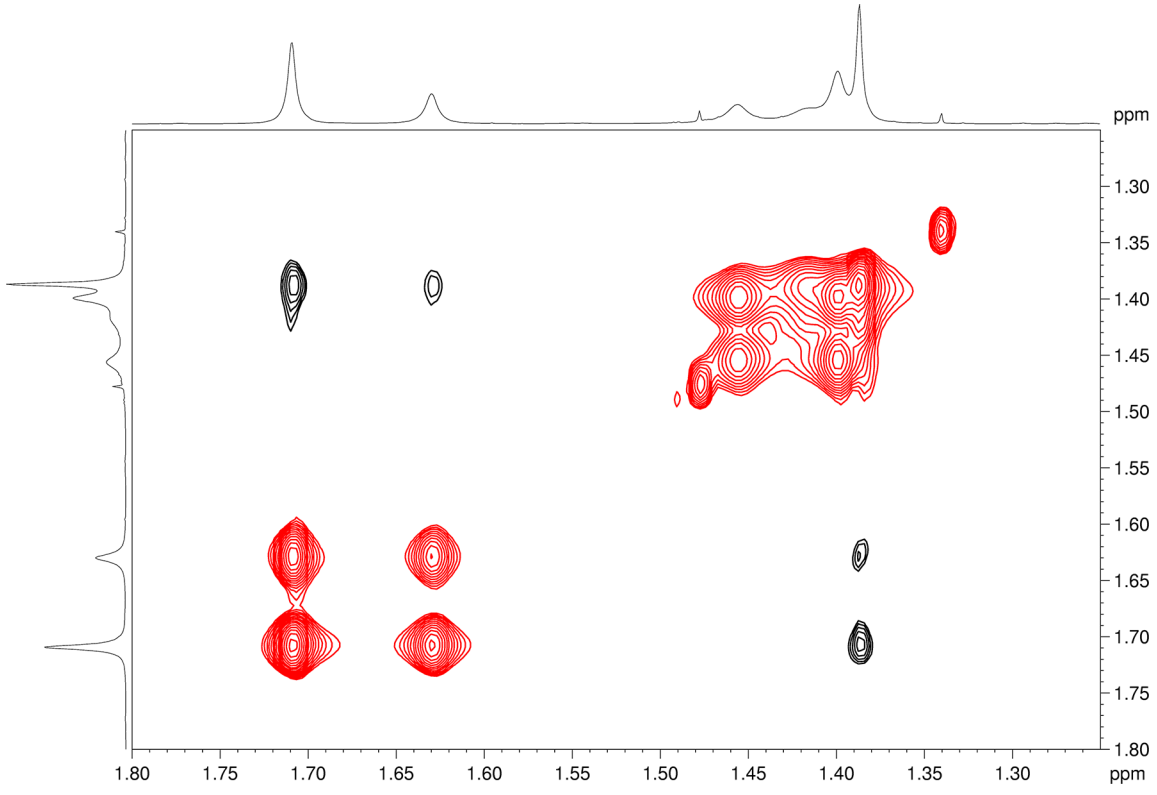

Figure 3. $^{1}H-^{1}H$ NOESY NMR spectrum of **3-Fe** recorded at 23 °C in C_7D_8.

conditions and with several solvents, this problem remained unresolved. To improve crystallinity and to explore the ability of **5-Fe** to act as a ligand, we then attempted to functionalize the N atom in **5-Fe** with a Lewis acid such as BF_3. Previous studies have established that $[(\eta^5\text{-}C_5Me_5)Fe(\eta^5\text{-}C_4H_4N)]$ and $[(\eta^5\text{-}C_4Me_4N)_2Fe](C_4Me_4NH)_2$ form stable BF_3 adducts.[11e,f,13] Kuhn also reported the formation of an Ag^+ adduct, $[Ag_2(\mu\text{-}\kappa N\text{-}(\eta^5\text{-}C_4Me_4N)_2Fe)_2](BF_2)\cdot 2MeOH$, on addition of $AgBF_4$ to $[(\eta^5\text{-}C_4Me_4N)_2Fe](C_4Me_4NH)_2$.[25] However, for **5-Fe** no adduct formation was observed with BF_3 or Ag^+, which is probably because of the effective steric shielding of the N atom from electrophilic attack. Instead, **5-Fe** is readily oxidized to [**5-Fe**][SbF_6] on addition of $AgSbF_6$ (see the Experimental Section for details).

This observation was surprising, since heteroferrocenes are more difficult to oxidize and heteroferrocenium cations are usually less stable than their carbocyclic counterparts.[11b,e,26] Decomposition pathways for azaferrocenium cations include nucleophilic attack or deprotonation at the 2,5-positions. Therefore, alkyl substitution at the sensitive 2,5-positions significantly increases the stability of the (di)azaferrocenium cations. Several electrochemical studies on the oxidation of azaferrocenes have been reported.[11b,e,26c] Furthermore, Nakashima and co-workers accomplished the chemical oxidation of azaferrocene, 2,5-dimethylazaferrocene, and 2,4-dimethylazafer-

dx.doi.org/10.1021/om400474e | *Organometallics* 2013, 32, 5887−5898

Scheme 3

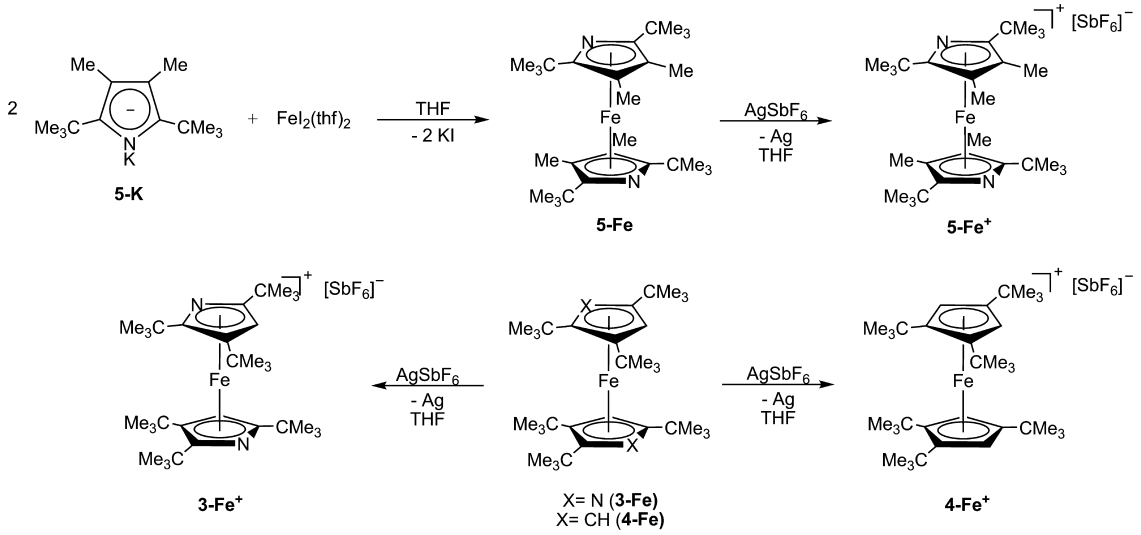

rocene with I_2 and characterized these species by several spectroscopic techniques, but no structural information is available on these complexes.[27]

Single crystals of [**5-Fe**][SbF_6] were grown by slow pentane diffusion into a CH_2Cl_2 solution, and the molecular structure is shown in Figure 4. Selected bond distances and angles are given in Table 2. The most notable feature is the elongated Pyr_{cent}–Fe bond of 1.76 Å in comparison to that in **3-Fe** (1.71 Å), which is comparable to the values obtained for $[\{\eta^5\text{-}1,2,3,4\text{-}C_5H(CHMe_2)_4\}_2Fe][BF_4]$ and $[\{\eta^5\text{-}1,2,4\text{-}C_5H_2(CHMe_2)_3\}_2Fe][BF_4]$.[28]

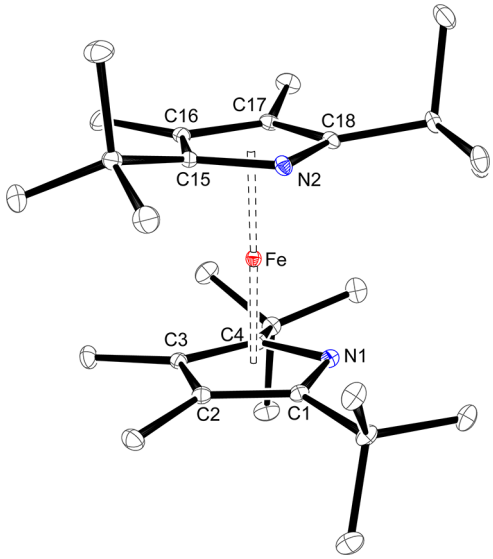

Figure 4. ORTEP diagram of **5-Fe**$^+$ with thermal displacement parameters drawn at the 50% probability level. The counteranion $[SbF_6]^-$ and the CH_2Cl_2 solvent are not shown. Selected bond lengths (Å) and angles (deg): Fe–N1 = 2.0801(15), Fe–C1 = 2.1303(17), Fe–C2 = 2.1765(17), Fe–C3 = 2.1399(18), Fe–C4 = 2.1056(17), Fe–N2 = 2.0829(15), Fe–C15 = 2.0940(17), Fe–C16 = 2.1507(17), Fe–C17 = 2.1852(18), Fe–C18 = 2.1345(17), N1–C4 = 1.390(2), N1–C4 = 1.390(2), C1–C2 = 1.435(2), C2–C3 = 1.427(3), C3–C4 = 1.433(2), N2–C15 = 1.392(2), N2–C18 = 1.387(2), C15–C16 = 1.433(2), C16–C17 = 1.426(2), C17–C18 = 1.435(2), Pyr_{cent}'–Fe = 1.76; pyr′–Fe–pyr′ = 178.5.

The more sterically encumbered derivatives **3-Fe** and **4-Fe** are also oxidized by $AgSbF_6$, yielding the corresponding (diaza)ferrocenium cations **3-Fe**$^+$ and **4-Fe**$^+$, respectively (Scheme 2; see the Experimental Section for details). The molecular structure of **4-Fe**$^+$ is shown in the Supporting Information, whereas Tables 1 and 2 give relevant structural details. However, slow degradation was observed for **3-Fe**$^+$ in CH_2Cl_2 solution to form a green solution and an off-white precipitate (vide infra). In $CHCl_3$ rapid decomposition of **3-Fe**$^+$ is observed.

Electrochemical Studies. Electrochemistry provides an ideal tool to investigate the electronic effect of isolobal CH versus N substitution.[29] Ferrocene derivatives undergo a reversible one-electron oxidation with fast electron transfer kinetics to form ferrocenium radical cations with significant chemical stability. In contrast, substitution of a CH group by a heteroatom increases the redox potentials but also decreases the stability of the heteroferrocenium cations in comparison to their carbocyclic counterparts (vide supra). Many studies have focused on stable azaferrocene derivatives[11b,e,26b,c] and diphosphaferrocenes.[26a,30] From these studies the following trends emerged: the replacement of one CH group by N changes the oxidation potential by +240–270 mV,[11b,e] and the exchange of two CH groups by P atoms induces a shift of +370 mV.[26a] In contrast, very little is known about the electrochemistry of diazaferrocenes;[10] Table 3 summarizes our results. Reversible Fe(II)/Fe(III) redox processes were observed for **1-Fe** and **5-Fe** (Figure 5), but degradation occurred for the most sterically demanding derivative **3-Fe** (see the Supporting Information for details). Simultaneously with the degradation of **3-Fe** a new reversible one-electron oxidation wave at $E_{1/2}$ = 1.00 V was detected, which was attributed to free pyrrole **3-H**. This assumption was further substantiated by an electrochemical study on **3-H**. Pyrroles can undergo one-electron oxidation, but the oxidized products are unstable toward nucleophilic attack at the 2,5-positions. However, the stability of the monocationic species increases when sterically demanding groups such as phenyl and *t*Bu protect these positions.[31] The electrochemical results for **3-Fe** point to an inherent instability of the diazaferrocenium species **3-Fe**$^+$ in CH_2Cl_2 solution (vide supra).

dx.doi.org/10.1021/om400474e | *Organometallics* 2013, 32, 5887–5898

Table 3. Electrochemical Potentials of Selected (Diaza)ferrocenes and Pyrroles vs SCE[a]

compd	$\Delta E_{1/2}$/V	solvent	ref
	(Diaza)ferrocenes		
$[(\eta^5\text{-}C_5H_5)_2Fe]$	0.46	CH_2Cl_2	32
1-Fe	0.76	CH_2Cl_2	this work
2-Fe	0.21	CH_2Cl_2	33
3-Fe	0.60[b]	CH_2Cl_2	this work
4-Fe	0.10	CH_2Cl_2	34
5-Fe	0.49	CH_2Cl_2	this work
	Pyrroles		
1-H	0.94	MeCN	31d
	1.12	CH_2Cl_2	this work
3-H	1.00	CH_2Cl_2	this work
5-H	0.91	CH_2Cl_2	this work

[a]Recorded in CH_2Cl_2 solution at ambient temperature (25 °C) with a scan rate of 0.10 V/s. **4-Fe** served as internal standard. [b]Degradation and formation of **3-H**.

In agreement with previous reports on azaferrocene,[11b,e,26b,c] the oxidation potential was shifted by +500−550 mV (i.e., 245−275 mV per CH group) when two CH groups were replaced by two N atoms. This value is in line with the observed anodic shift (ca. +0.5 V) for **1-Co** in comparison to $[(\eta^5\text{-}C_5H_5)_2Co]$.[15a]

Mössbauer Spectroscopic Studies. Ferrocene is not only an iconic molecule in the development of organometallic chemistry, but it was also the first organometallic compound to be studied by Mössbauer spectroscopy more than 50 years ago.[35] Since then, many ferrocene derivatives have been investigated with respect to their hyperfine parameters, whereas data on diazaferrocenes are missing. Electronic effects of the ring substituents exhibit only a minor influence on the isomer shift, δ. However, the quadrupole splitting, ΔE_Q, shows some degree of sensitivity to the ring substitution pattern and can also be used for example to evaluate the distortion from the parallel ring arrangement.[36] These observations can be explained by the molecular orbital (MO) description of ferrocene.[37] The ΔE_Q parameter in iron sandwich complexes depends on the relative populations of the e_{2g} ($d_{x^2-y^2}$, d_{xy}) and e_{1g} (d_{xz}, d_{yz}) orbitals (in D_{5d} symmetry), whereas the contribution of the fully occupied d_{z^2} orbital is usually neglected when ΔE_Q values are compared. However, the e_2 and e_1 orbitals contribute differently to the electric field gradient according to $\Delta E_Q \propto 2p_2 - p_1$, where p_2 and p_1 represent the electronic populations of the e_2 and e_1 MOs, respectively. The large ΔE_Q splitting for ferrocene (2.45 mm s^{-1})[38] is attributable to the filled and largely unperturbed e_2 levels, giving rise to very different e_2 and e_1 populations. Very similar ΔE_Q parameters of ferrocene and azaferrocene (2.49 mm s^{-1})[38,39] suggest that the populations of the MOs are not much altered when one CH group is replaced by an N atom (Table 4). In contrast, mono- and diphosphaferrocenes generate much lower ΔE_Q values as a result of significant orbital mixing between the $d_{x^2-y^2}$ and d_{z^2} orbitals.[40] However, the most pronounced effect on the ΔE_Q parameter is observed when ferrocene is oxidized to ferrocenium, which causes an almost complete collapse of the ΔE_Q value ($\Delta E_Q \approx 0.1-0.6$ mm s^{-1}) and a significant asymmetric line broadening attributed to spin−lattice relaxation processes.[41]

We recorded ^{57}Fe Mössbauer spectra for our diazaferrocene derivatives at $T \approx 100$ K, and these results are given in Table 4. For comparison, we also included the carbocyclic derivatives **2-Fe** and **4-Fe**. The ^{57}Fe Mössbauer spectra of the diamagnetic Fe(II) low-spin diazaferrocenes **1-Fe**, **3-Fe**, and **5-Fe** are shown in Figure 6 and consist of well-resolved doublets with line widths Γ_{fwhm} on the order of the experimental line width of the spectrometer used ($\Gamma_{exp} \approx 0.22$ mm s^{-1}). The δ and ΔE_Q parameters are relatively insensitive to the ring-substitution pattern, and the numerical values for ferrocene and diazaferrocene derivatives suggest very similar electronic structures at the ^{57}Fe nucleus in these complexes (Table 4).

When diazaferrocene **5-Fe** is oxidized to [**5-Fe**][SbF_6], ΔE_Q collapses and a single, broad asymmetric line is detected in the ^{57}Fe Mössbauer spectrum (Figure 7). The spectrum was analyzed on the basis of the model reported by Blume and Tjon, which considers a fluctuating magnetic field parallel to

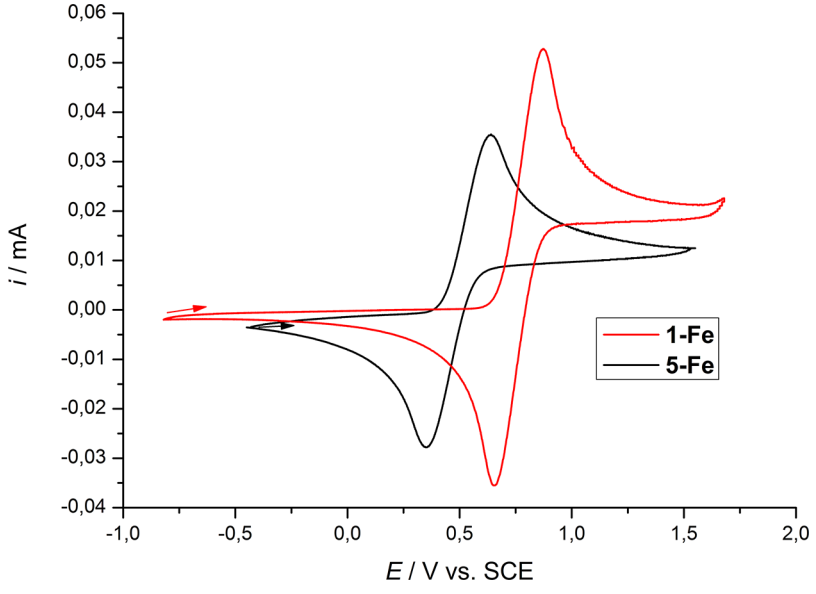

Figure 5. Cyclic voltammograms (CV) for **1-Fe** and **5-Fe**, recorded at ambient temperature in CH_2Cl_2 with 0.1 M [*n*-Bu_4N][PF_6] supporting electrolyte and a scan rate of 100 mV/s.

dx.doi.org/10.1021/om400474e | *Organometallics* 2013, 32, 5887−5898

Table 4. ^{57}Fe Mössbauer Spectroscopic Data for Several (Diaza)ferrocene and (Diaza)ferrocenium Complexes[a]

compd	δ/mm s^{-1} [Γ_{fwhm}/mm s^{-1}]	ΔE_Q/mm s^{-1}	ref
$[(\eta^5\text{-}C_5H_5)_2Fe]$	0.54	2.45	38
	0.53[b]	2.40[b]	42
$[(\eta^5\text{-}C_5H_5)_2Fe][BF_4]$	0.61		41b
$[(\eta^5\text{-}C_5H_5)Fe(\eta^5\text{-}C_4H_4N)]$	0.59	2.49	38, 39
$[(\eta^5\text{-}C_5H_5)Fe(\eta^5\text{-}C_4H_4N)][I_3]$	0.43[b]	0.75[b]	27
$[(\eta^5\text{-}C_5H_5)Fe(\eta^5\text{-}C_4H_4P)]$	0.51	2.07	43
$[(\eta^5\text{-}C_4H_4P)_2Fe]$	0.50	1.79	44
1-Fe	0.63 [0.27]	2.54	this work
2-Fe	0.57[b]	2.54[b]	42
3-Fe	0.70 [0.24]	2.65	this work
[**3-Fe**][SbF_6][c]	0.69 [0.44][d]	−0.05[d]	this work
5-Fe	0.66 [0.26]	2.58	this work
[**5-Fe**][SbF_6]	0.66 [0.32][d]	−0.08[d]	this work

[a]Recorded in the solid state on powdered samples at ca. 100 K. Isomer shifts were determined relative to α-iron at 298 K and were not corrected in terms of second-order Doppler effects. [b]Recorded at 80 K. [c]In addition to [**3-Fe**][SbF_6] (88%), another unidentified species (12%) was also present in the sample (δ = 1.22 mm s^{-1}, ΔE_Q = 2.34 mm s^{-1}). [d]The Mössbauer spectrum was analyzed and simulated on the basis of the model as outlined in ref 45 (see text).

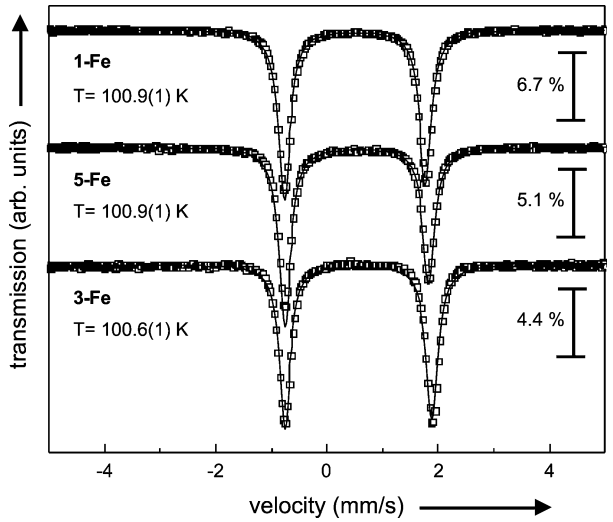

Figure 6. ^{57}Fe Mössbauer spectra of **1-Fe**, **3-Fe**, and **5-Fe**. The significant intensity asymmetry (A^-/A^+= 1.22) of the doublet for **5-Fe** may be attributable to texture effects in the sample. The data were fitted to Lorentzian lines, with line position, full width at half-maximum (fwhm), and intensity as free parameters (solid lines).

the electric field gradient axis.[45] Because of a significant correlation between the internal magnetic field B at the ^{57}Fe nucleus site and the fluctuation rate of the magnetic field vector ν_c, the spectrum was simulated with an fixed internal magnetic field of B = 42.5 T, whereas the line position, full width at half-maximum, intensity, and magnetic field fluctuation rate were free parameters. One should note that Abraham et al. determined from Mössbauer measurements on $[(\eta^5\text{-}C_5H_5)_2Fe][BF_4]$ at T = 4.2 K with an applied external magnetic field of B_{ext} = 5.5 T an internal magnetic field of B = 42.5 T.[41c] On the basis of this assumption, a fluctuation rate of ν_c = 96 MHz for [**5-Fe**][SbF_6], an isomer shift of δ = 0.66 mm s^{-1}, and a quadrupole splitting of ΔE_Q = −0.08 mm s^{-1} were

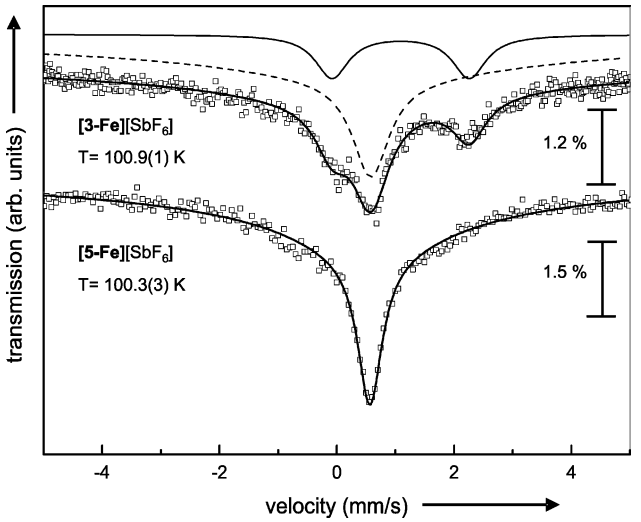

Figure 7. ^{57}Fe Mössbauer spectra of [**3-Fe**][SbF_6] and [**5-Fe**][SbF_6]. The Mössbauer spectra were analyzed and simulated on the basis of the model as outlined in ref 45 (solid lines). In the case of [**3-Fe**][SbF_6], two nonequivalent ^{57}Fe sites were considered as described in the text. The subspectra of these two species were plotted and arranged with a marginal shift against the transmission axis.

determined. In addition, the Mössbauer spectrum of a freshly prepared sample of [**3-Fe**][SbF_6] shows two different species in a ratio of ca. 88:12. The Mössbauer parameters of the major species were also computed by use of the Blume−Tjon model[45] with a fixed internal magnetic field of B = 42.5 T and are consistent with the expected diazaferrocenium cation (δ = 0.69 mm s^{-1}, ΔE_Q = −0.05 mm s^{-1}) with a fluctuation rate of ν_c = 57 MHz, whereas the minor species (12%) exhibits a well-resolved doublet with δ = 1.22 mm s^{-1} and ΔE_Q = 2.34 mm s^{-1}). The latter parameters were determined by a simple fit to Lorentzian lines and suggest the presence of an Fe(II) high-spin (S = 2) species in the material and is probably a result of the inherent instability of [**3-Fe**][SbF_6] (vide supra).

We have also evaluated the same sample by EPR spectroscopy, and found two signals at $g_{\|}$ = 4.03 and $g_{\perp}$ = 1.60 (at 5 K; Figure 8), which are consistent with an $^2E_{2g}$ ($e_{2g}^3a_{1g}^2$) ground state and similar to those obtained for several ferrocenium derivatives.[46] No other resonances are observed, consistent with the Mössbauer result, confirming that the minor species (14%, δ = 1.25 mm s^{-1}, ΔE_Q = 2.31 mm s^{-1}) is indeed a high-spin (S = 2) Fe(II) complex.

Density Functional Theory (DFT) Studies. Density functional theory (DFT) computations are a very convenient tool to evaluate (at low computational costs in comparison to post-Hartree−Fock methods) the electronic structure of larger molecules and clusters of low symmetry.[47] Unfortunately, the exact functional of the electron density is unknown and only approximate expressions are available, and this usually requires an exhaustive evaluation of different density functionals (DFs) to identify the best option for a given problem. In previous studies we have evaluated a series of modern hybrid and hybrid-meta DFs and found that the best agreement between experimental and calculated structures is obtained with the dispersion-corrected B97 functional, B97D.[48] We focused on the most sterically encumbered derivatives, **3-Fe** and **4-Fe**, in an attempt to gain some additional insights into the bonding of these molecules. The DFT calculations reproduce well the solid-state molecular structures of **3-Fe** and **4-Fe** (see the

dx.doi.org/10.1021/om400474e | Organometallics 2013, 32, 5887−5898

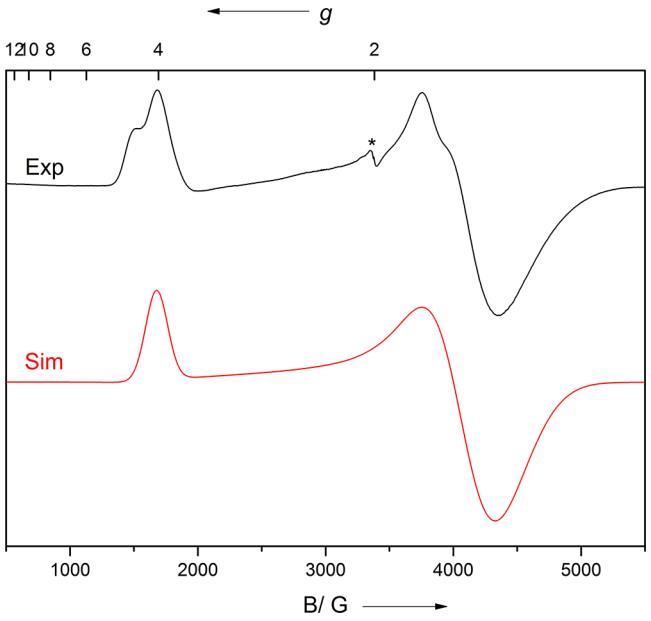

Figure 8. X-band EPR spectrum recorded at 5 K on a powdered sample of [**3-Fe**][SbF_6] (9.4837 GHz, 13 mW/12 dB, modulation frequency 100 kHz, modulation amplitude 10 G). Only the major species was simulated, and the signal marked with an asterisk (*) corresponds to an impurity in the probe cavity. The minor species is probably due to a rotational isomer (see discussion of the dynamic NMR behavior of **3-Fe**).

Supporting Information for details). Selected Kohn–Sham orbitals of these molecules are shown in Figure 9. The major differences are the relative stabilization of the HOMOs and LUMOs in **3-Fe** and the mixing between the $d_{x^2-y^2}$ and d_{z^2} orbitals (HOMO and HOMO-2), whereas no mixing is observed in **4-Fe**. However, the HOMO–LUMO gaps in both molecules are very similar, consistent with their UV–vis data (see the Supporting Information for details).

The variable-temperature ^{1}H NMR studies on **3-Fe** and **4-Fe** suggested that the Pyr–Fe bonds are slightly stronger than the corresponding Cp–Fe bonds. To evaluate the mechanical strength of bonds between two atoms, the concept of compliance constants has been introduced,[49] which allows different molecular surroundings to be compared. Table 5 gives the values for the relaxed force constants f (reciprocal compliance constants) for the averaged Pyr/Cp–Fe bonds in **3-Fe**/**3-Fe**$^+$ and **4-Fe**/**4-Fe**$^+$, respectively. On the basis of these data the Fe–Pyr bonds are stronger than in the corresponding ferrocene derivatives, consistent with the results of He I photoelectron studies on **1-Fe** and **2-Fe**.[9c] Furthermore, on oxidation the Fe–Pyr bonds in **3-Fe**$^+$ become significantly weaker than those of the neutral **3-Fe**.

CONCLUSIONS

We have prepared several sterically encumbered diazaferrocenes and provided a detailed investigation of the electronic and molecular structure of these diazaferrocenes and their ferrocene analogues. Diazaferrocenes **1-Fe** and **3-Fe** have molecular structures very similar to those of their ferrocene derivatives **2-Fe** and **4-Fe**, respectively. However, despite the steric demand of pyrrolyl **3** being comparable to that of cyclopentadienyl **4**, no iron half-sandwich complexes such as [{η^5-2,3,5-(Me_3C)$_3$$C_4$HN}FeI]$_2$ (**3-FeI**) can be isolated; instead, the thermodynamically favored diazaferrocene (**3-Fe**) is obtained. This is probably because of the ready ability of pyrrolyl to undergo η^5–κ^1 haptotropic shifts in the half-sandwich intermediate and the thermodynamic stability of **3-Fe** with strong Pyr–Fe bonds. Interestingly, **3-Fe** exhibits a rather large rotation barrier in solution and two interconverting rotational isomers of similar free energy, ΔG(298 K) = 0.3 kcal mol^{-1}, are observed in solution by NMR spectroscopy. Because of the *t*Bu groups in the 2,5-positions of the pyrrolyl system, the N atoms of the diazaferrocene are effectively shielded and cannot be further functionalized by electrohiles such as BF_3 and Ag^+. However, on addition of $AgSbF_6$ **3-Fe** and **5-Fe** are oxidized to the corresponding diazaferrocenium cations **3-Fe**$^+$ and **5-Fe**$^+$. Electrochemical studies revealed that the replacement of two CH groups in ferrocene by two N atoms significantly shifts the oxidation potential by +500–550 mV, consistent with the energetic stabilization of the diazaferrocene HOMO in comparison to that of ferrocene. While reversible electrochemical oxidation is observed for the diazaferrocenes **1-Fe** and **5-Fe**, the most sterically encumbered derivative **3-Fe** shows decomposition and the formation of pyrrole **3-H** under the same conditions. However, EPR spectroscopy confirmed an $^2E_{2g}$ ground state for diazaferrocenium **3-Fe**$^+$. In addition, Mössbauer investigations establish that the electronic structures at the ^{57}Fe nucleus are very similar in the diazaferrocene and ferrocene complexes. The $^2E_{2g}$ ground state for **3-Fe**$^+$ was confirmed by EPR spectroscopy. DFT calculations on **3-Fe** and **4-Fe** establish that frontier orbitals are related, but for diazaferrocene **3-Fe** mixing between the d_{z^2} and $d_{x^2-y^2}$ orbitals occurs. In addition, relaxed force constants indicate that the mechanical strength of the Fe–Pyr bonds is stronger than that of the Fe–Cp bonds.

In conclusion, this study suggests that an even more sterically demanding pyrrolyl ligand might be required to accomplish the effective stabilization of the half-sandwich intermediate. Furthermore, we are currently exploring the ability of pyrrollyl **3** to isolate other transition-metal half-sandwich complexes, in which it can undergo η^5–κ^1 haptotropic shifts. These results will be reported in due course.

EXPERIMENTAL SECTION

General Considerations. All synthetic and spectroscopic manipulations were carried out under an atmosphere of prepurified nitrogen or argon, either in a Schlenk apparatus or in a glovebox. Solvents were dried and deoxygenated either by distillation under a nitrogen atmosphere from sodium benzophenone ketyl (THF) or by an MBraun GmbH solvent purification system. NMR spectra were recorded on a Bruker DPX 200, Bruker DRX 400, Bruker Avance III 400, or Bruker Avance II 300 spectrometer at ambient temperature unless stated otherwise. The chemical shifts are expressed in parts per million (ppm) and are referenced to residual ^{1}H or ^{13}C of the solvent or tetramethylsilane (δ_H 7.16 for benzene, 5.32 for dichloromethane, 2.08 for toluene (CH_3)) for the ^{1}H spectra and the solvent signal (δ_C 128.0 ppm for benzene, 53.8 for dichloromethane, 20.4 for toluene (CH_3)) for the ^{13}C spectra. The assignment follows the numbering

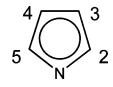

A Bruker Vertex 70 spectrometer was used for recording IR spectra. Elemental analyses were performed by combustion and gas chromatographic analysis with an Elementar varioMICRO instrument. Mass spectrometry was carried out on a Finnigan MAT 90 X instrument (EI). UV–vis spectra were recorded on a Varian Cary 50 Scan instrument. Cyclic voltammograms were recorded on a Metrohm μAutolab Type III potentiostat/

dx.doi.org/10.1021/om400474e | *Organometallics* 2013, 32, 5887–5898

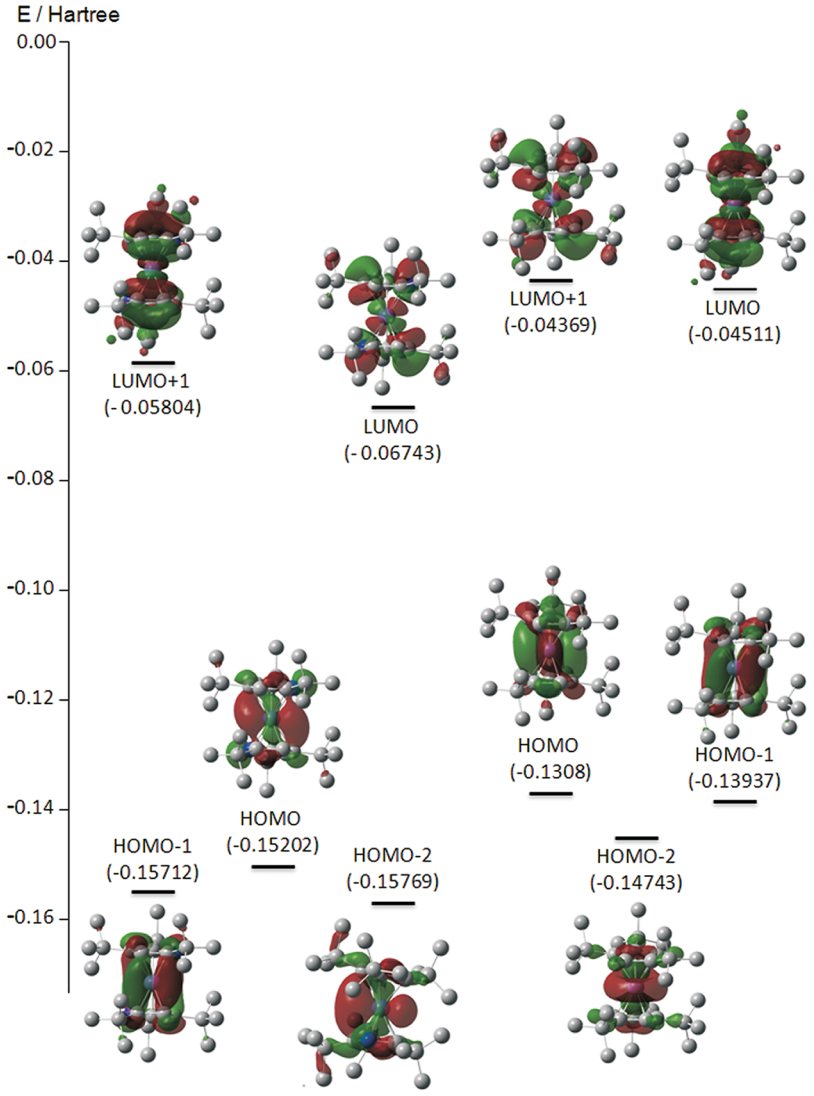

Figure 9. Selected Kohn–Sham orbitals (B97D, 6-311G(d,p)) of **3-Fe** (left) and **4-Fe** (right) (with imposed C_2 symmetry).

Table 5. Relaxed Force Constants for Averaged Fe-Pyr/Cp Bonds in 3-Fe/3-Fe$^+$ and 4-Fe/4-Fe$^+$

compd	relaxed force constant f/N cm^{-1}
3-Fe	1.38
3-Fe$^+$	0.98
4-Fe	1.26
4-Fe$^+$	1.00

galvanostat in a CH_2Cl_2 solution containing 0.1 M [*n*-Bu_4N][PF_6] as supporting electrolyte. A 99.9% platinum wire (φ 0.6 mm, Chempur) was used for the working and counter electrodes, respectively, and the potentials were measured against a 99.9% silver wire (φ 0.6 mm, Chempur). Redox potentials were calculated using the formula $\Delta E_{1/2} = {}^1/_2(E_p^{ox} + E_p^{red})$, where E_p^{ox} and E_p^{red} are peak potentials. The couple $[(\eta^5\text{-}C_5H_5)_2Fe]^+/[(\eta^5\text{-}C_5H_5)_2Fe]$ displayed a reversible cyclic voltammetric trace with the redox potential $\Delta E_{1/2}$ = +0.46 V (in CH_2Cl_2) under these conditions.[32]

Mössbauer Studies. ^{57}Fe Mössbauer spectroscopic measurements have been performed on an absorber with an area density corresponding to about 0.06–0.12 mg of ^{57}Fe/cm^2. A conventional transmission spectrometer with sinusoidal velocity sweep was used. The source was about 10 mCi of ^{57}Co in a rhodium matrix kept at room temperature. The absorber containers were made of Teflon and were fixed within copper clamps. After installation of the samples the chamber was evacuated and flushed five times with N_2 gas and during the data collection the N_2 pressure was kept at ca. 10 mbar. Temperature control and measurement were performed with a Lakeshore 336-T controller using a calibrated Si diode attached to the copper clamp. Isomer shifts (δ) were determined relative to α-iron at 298 K but were not corrected for second-order Doppler effects.

EPR Studies. The X-band EPR spectra were recorded on a Bruker EMX spectrometer at 5 K, and the spectra were simulated with EasySpin 4.5.0.[50]

X-ray Diffraction Studies. Single crystals of each compound were examined in inert oil. Data collection was performed on various Oxford Diffraction diffractometers using monochromated Mo Kα or mirror-focused Cu Kα radiation (Table 1). Absorption corrections were performed on the basis of multiscans. The data were analyzed using the SHELXL97 program.[51] In all cases, the non-hydrogen atoms were refined anisotropically. *Special features*: **3-Fe** was refined as a racemic twin.

Materials. THF, diethyl ether, hexamethyldisiloxane, hexanes, and benzene were distilled over sodium. CH_2Cl_2 and acetonitrile were dried over CaH_2. All other solvents were purified and dried by a solvent purification system from MBraun and stored over molecular sieves (4A) under nitrogen. Other reagents were used as received. K(Pyr^{tBu2}) (**1-K**) was prepared from KH and **1-H** in tetrahydrofuran.

dx.doi.org/10.1021/om400474e | *Organometallics* 2013, 32, 5887–5898

K(Pyr^{tBu3}) (**3-K**),[19] K($Pyr^{tBu2Me2}$) (**5-K**),[19] $FeI_2(thf)_2$,[52] and $FeCl_2$[53] were prepared according to literature procedures.

Synthesis of [(η^5-2,3,5-(Me_3C)$_3C_4HN$)$_2$Fe] (3-Fe). The pyrrolide **3-K** (0.500 g, 1.83 mmol) dissolved in THF (20 mL) was added at ambient temperature to a solution of $FeI_2(thf)_2$ (0.415 g, 0.92 mmol) in THF (25 mL). The reaction mixture turned purple and was stirred for 12 h and then filtered through Celite. The solvent was removed under dynamic vacuum, and the residue was extracted with pentane. Evaporation of the solvent gave a purple powder. Yield: 0.275 g (0.52 mmol, 57%). Crystals of **3-Fe** suitable for X-ray analysis were obtained from a saturated hexamethyldisiloxane solution at −30 °C. Purification of **3-Fe** was also accomplished by sublimation at 150 °C under dynamic vacuum (0.01 mbar). Mp: >250 °C dec. Anal. Calcd for $C_{32}H_{56}N_2Fe$: C, 73.26; H, 10.76; N, 5.34. Found: C, 73.25; H, 10.59; N, 5.27. The NMR data were consistent with two C_2-symmetric isomers, which exchanged on the NMR time scale. Two sets of resonances corresponding to the two rotational isomers were observed in the $^{13}C\{^1H\}$ NMR spectrum. Although an accurate assignment was difficult, the chemical shifts were as follows. $^{13}C\{^1H\}$ NMR (400 MHz, C_7D_8, 298 K): δ 112.9 (C_q, Pyr), 112.5 (Cq, Pyr), 110.7 (C_q, Pyr), 100.1 (C_q, Pyr), 67.3 (CH, Pyr), 66.4 (CH, Pyr), 34.9 ($C(CH_3)_3$), 34.10 ($C(CH_3)_3$), 33.7 ($C(CH_3)_3$), 33.3 ($C(CH_3)_3$), 33.2 ($C(CH_3)_3$), 32.8 ($C(CH_3)_3$), 32.6 ($C(CH_3)_3$), 31.7 ($C(CH_3)_3$), 31.2 ($C(CH_3)_3$). The EI mass spectrum (70 eV) showed a molecular ion at m/z 524 with the following isotopic cluster distribution for $C_{32}H_{56}N_2Fe$ (calcd %, obsd %): 522 (6, 6), 523 (2, 3), 524 (100, 100), 525 (38, 40), 526 (7, 8), 527 (1, 1).

Synthesis of [(η^5-2,3,5-(Me_3C)$_3C_4HN$)$_2$Fe][SbF_6] (3-Fe$^+$). $AgSbF_6$ (0.077 mg, 0.23 mmol) was added with stirring to a CH_2Cl_2 solution of **3-Fe** (0.118 g, 0.23 mmol). Immediately, the reaction mixture turned from purple-red to brownish green and a precipitate was formed. After 1.5 h the mixture was filtered and concentrated to ca. 2 mL. Pentane (10 mL) was added to the stirred CH_2Cl_2 solution, causing the precipitation of a green powder, which was filtered, washed with pentane (2 × 2 mL), and dried in vacuo. Yield: 113 mg (0.14 mmol, 60%). Mp: 131−136 °C. Anal. Calcd for $C_{32}H_{56}N_2FeSbF_6$: C, 50.55; H, 7.42; N, 3.68. Calcd for $C_{32}H_{56}N_2FeSb_6\cdot 0.33CH_2Cl_2$: C, 49.24; H, 7.24; N, 3.55. Found: C, 48.16; H, 7.10; N, 3.35. The ^1H NMR spectrum recorded in $CDCl_3$ showed the presence of CH_2Cl_2 (δ 5.31). ^1H NMR (200 MHz, CD_2Cl_2, 298 K): δ −2.0 ($C(CH_3)_3$, $\nu_{1/2}$ = 180 Hz), −9.2 ($C(CH_3)_3$, $\nu_{1/2}$ = 200 Hz), −10.7 (very broad, signal overlap), −11.8 ($C(CH_3)_3$, $\nu_{1/2}$ = 200 Hz) ppm.

Synthesis of [(η^5-1,2,4-(Me_3C)$_3C_5H_2$)$_2$Fe][SbF_6] (4-Fe$^+$). Addition of $AgSbF_6$ (0.062 mg, 0.18 mmol) to a stirred solution of **4-Fe** (0.100g, 0.18 mmol) in CH_2Cl_2 induced an immediate color change from red to brownish green and precipitation of silver. After it was stirred for 1 h at ambient temperature, the mixture was filtered and a layer of pentane was added on top of the CH_2Cl_2 solution. After several days of slow diffusion large brown-green crystals of **4-Fe**$^+$ were isolated. Yield: 0.104 g (0.14 mmol, 78%). Mp: >300 °C dec. Anal. Calcd for $C_{34}H_{56}FeSbF_6$: C, 53.99; H, 7.46. Found: C, 53.98; H, 7.58. ^1H NMR (200 MHz, CD_2Cl_2, 298 K): δ −4.6 ($C(CH_3)_3$, broad), −9.7 ($C(CH_3)_3$) ppm. Both ^1H NMR resonances showed significant overlap.

Synthesis of [(η^5-2,5-(Me_3C)$_2$-3,4-Me_2C_4N)$_2$Fe] (5-Fe). A solution of **5-K** (0.150 g, 0.62 mmol) in THF (5 mL) was added at room temperature to a suspension of $FeCl_2$ (0.039 g, 0.31 mmol) in THF (10 mL). The solution turned red and was stirred overnight. The solvent was removed under dynamic vacuum, and the residue was extracted with pentane. Evaporation of the solvent gave a red residue that was recrystallized from a saturated hexamethyldisiloxane solution at −24 °C to give red crystals. Yield: 0.100 g (0.20 mmol, 65%). Mp: 176 °C. Anal. Calcd for $C_{28}H_{48}N_2Fe$: C, 71.78; H, 10.33; N, 5.98. Found: C, 71.65; H, 10.45; N, 5.71. ^1H NMR (200 MHz, C_6D_6, 298 K): δ 1.80 (s, 12H, CH_3), 1.53 (s, 36H, $C(CH_3)_3$) ppm. $^{13}C\{^1H\}$ NMR (50 MHz, C_6D_6, 298 K): δ 110.1 (C_q, C-3/-4), 82.3 (C_q, C-2/-5), 33.1 ($C(CH_3)_3$), 30.7 ($C(CH_3)_3$), 12.3 (CH_3,) ppm. The EI mass spectrum (70 eV) showed a molecular ion at m/z 486 with the following isotopic cluster distribution for $C_{28}H_{48}N_2Fe$ (calcd %, obsd %): 466 (6, 6), 467 (3, 2), 468 (100, 100), 469 (31, 35), 470 (6, 6), 471 (1, 1).

Synthesis of [(η^5-2,5-(Me_3C)$_2$-3,4-Me_2C_4N)$_2$Fe][SbF_6] (5-Fe$^+$). With stirring $AgSbF_6$ (0.036 mg, 0.11 mmol) was added to a solution of **5-Fe** (0.050 g, 0.11 mmol) in CH_2Cl_2. Immediately, the reaction mixture turned from red to green and a precipitate was formed. After it was stirred for 1 h at ambient temperature, the mixture was filtered and concentrated and a layer of pentane was added on top of the green CH_2Cl_2 solution. After several days of slow diffusion large green crystals of **5-Fe**$^+$ were isolated. Yield: 0.036 g (0.05 mmol, 45%). Mp: 128 − 136 °C dec (with color change from green to dark brown). ^1H NMR (300 MHz, CD_2Cl_2, 298 K): δ −12.3 (36H, $C(CH_3)_3$), $\nu_{1/2}$ = 365 Hz), −37.7 (12H, CH_3, $\nu_{1/2}$ = 660 Hz) ppm. Anal. Calcd for $C_{28}H_{48}N_2FeSbF_6$: C, 47.75; H, 6.87; N, 3.98. Found: C, 47.64; H, 6.81; N, 3.74.

Computational Details. All calculations employed the long-range dispersion-corrected Grimme functional (B97D)[48] and were carried out with Gaussian 09.[54] No symmetry restrictions were imposed (C_1). C, H, N, and Fe were represented by an all-electron 6-311G(d,p) basis set. The nature of the extrema (minima) was established with analytical frequency calculations. The zero-point vibration energy (ZPE) and entropic contributions were estimated within the harmonic potential approximation. The Gibbs free energy, ΔG, was calculated for T = 298.15 K and 1 atm. Geometrical parameters were reported within an accuracy of 10^{-3} Å and 10^{-1} deg.

■ ASSOCIATED CONTENT

Supporting Information

CIF files, figures, and tables giving crystallographic data, (VT) ^1H NMR spectra of **3-Fe**, the molecular structure of [**4-Fe**][SbF_6], synthesis and solid-state magnetic susceptibility vs T data for [**4-Fe**][BF_4], IR spectra, the Mössbauer spectrum of **3-Fe** after exposure to air for 1 week, UV/vis spectroscopic data, and computational details. This material is available free of charge via the Internet at http://pubs.acs.org. CCDC numbers: 940434 (**3-Fe**), 940435 ([**4-Fe**][SbF_6]), 940436 ([**5-Fe**]-[SbF_6]·CH_2Cl_2).

■ AUTHOR INFORMATION

Corresponding Author

*E-mail for M.D.W.: mwalter@tu-bs.de.

Present Address

†Westfälische Wilhelms-Universität Münster, Organisch-Chemisches Institut, Corrensstrasse 40, 48149 Münster, Germany.

Author Contributions

The manuscript was written through contributions of all authors and all authors have given approval to the final version of the manuscript.

Notes

The authors declare no competing financial interest.

■ ACKNOWLEDGMENTS

MDW gratefully acknowledges the financial support by the Deutsche Forschungsgemeinschaft (DFG) through the Emmy-Noether program (WA 2513/2-1 and WA 2513/2-2). We thank the Department of Physics (IPKM) of the TU Braunschweig and in particular Prof. F. J. Litterst for using the equipment.

■ REFERENCES

(1) (a) Kealy, T. P.; Pauson, P. L. *Nature* **1951**, *168*, 1039. (b) Wilkinson, G.; Rosenblum, M.; Whiting, M. C.; Woodward, R. B. *J. Am. Chem. Soc.* **1952**, *74*, 2125. (c) Wilkinson, G.; Cotton, F. A. *Prog. Inorg. Chem.* **1959**, *1*, 1. (d) Werner, H. *Angew. Chem., Int. Ed.* **2012**, *51*, 6052.

(2) (a) Janiak, C.; Schumann, H. *Adv. Organomet. Chem.* **1991**, *33*, 291. (b) *Comprehensive Organometallic Chemistry II*; Abel, E. W., Stone, F. G. A., Wilkinson, G., Eds.; Pergamon: New York, 1995. (c) *Comprehensive Organometallic Chemistry*; Wilkinson, G., Stone, F. G. A., Abel, E. W., Eds.; Pergamon: New York, 1982.
(3) (a) Gladysz, J. A. *Chem. Rev.* **2000**, *100*, 1167 (introduction to the special issue "Frontiers in Metal-Catalyzed Polymerization"). (b) Chirik, P. J. *Organometallics* **2010**, *29*, 1500. (c) Werkema, E. L.; Andersen, R. A. *J. Am. Chem. Soc.* **2008**, *130*, 7153. (d) Werkema, E. L.; Maron, L.; Eisenstein, O.; Andersen, R. A. *J. Am. Chem. Soc.* **2007**, *129*, 2529. (e) Werkema, E. L.; Messines, E.; Perrin, L.; Maron, L.; Eisenstein, O.; Andersen, R. A. *J. Am. Chem. Soc.* **2005**, *127*, 7781. (f) Maron, L.; Werkema, E. L.; Perrin, L.; Eisenstein, O.; Andersen, R. A. *J. Am. Chem. Soc.* **2004**, *127*, 279. (g) Zi, G.; Blosch, L. L.; Jia, L.; Andersen, R. A. *Organometallics* **2005**, *24*, 4602. (h) Golden, J. T.; Andersen, R. A.; Bergman, R. G. *J. Am. Chem. Soc.* **2001**, *123*, 5837.
(4) (a) *Chiral Ferrocenes in Asymmetric Catalysis*; Dai, L.-X., Hou, X.-L., Eds.; Wiley-VCH: Weinheim, Germany, 2010. (b) *Ferrocenes: homogeneous catalysis, organic synthesis, materials science*; Togni, A., Hayashi, T., Eds.; VCH: Weinheim, Germany, 1995. (c) *Metallocenes: synthesis reactivity applications*; Togni, A., Haltermann, R. L., Eds.; Wiley-VCH: Weinheim, Germany, 1998. (d) Hartwig, J. F. *Organotransition Metal Chemistry: From Bonding to Catalysis*; University Science: Sausalito, CA, 2010.
(5) Kuhn, N. *Bull. Soc. Chim. Belg.* **1990**, *99*, 707.
(6) (a) Joshi, K. K.; Pauson, P. L.; Qazi, A. R.; Stubbs, W. H. *J. Organomet. Chem.* **1964**, *1*, 471. (b) King, R. B.; Bisnette, M. B. *Inorg. Chem.* **1964**, *3*, 796. (c) Efraty, A.; Jubran, N.; Goldman, A. *Inorg. Chem.* **1982**, *21*, 868.
(7) (a) Tille, D. *Z. Anorg. Allg. Chem.* **1972**, *390*, 234. (b) Kuhn, N.; Horn, E. M. *Inorg. Chim. Acta* **1990**, *170*, 155.
(8) Reagen, W. K.; Radonovich, L. J. *J. Am. Chem. Soc.* **1987**, *109*, 2193.
(9) (a) Seel, F.; Sperber, V. *Angew. Chem.* **1968**, *80*, 38. (b) Seel, F.; Sperber, V. *J. Organomet. Chem.* **1968**, *14*, 405. (c) Janiak, C.; Kuhn, N.; Gleiter, R. *J. Organomet. Chem.* **1994**, *475*, 223.
(10) Love, J. B.; Salyer, P. A.; Bailey, A. S.; Wilson, C.; Blake, A. J.; Davies, E. S.; Evans, D. J. *Chem. Commun.* **2003**, 1390.
(11) (a) Kowalski, K.; Zakrzewski, J. *J. Organomet. Chem.* **2004**, *689*, 1046. (b) Kowalski, K.; Winter, R. F. *J. Organomet. Chem.* **2008**, *693*, 2181. (c) Kowalski, K. *Coord. Chem. Rev.* **2010**, *254*, 1895. (d) Kovač, B.; Kowalski, K.; Novak, I. *J. Organomet. Chem.* **2011**, *696*, 1664. (e) Brunker, T. J.; Roembke, B. T.; Golen, J. A.; Rheingold, A. L. *Organometallics* **2011**, *30*, 2272. (f) Brunker, T. J.; Kovac, B.; Kowalski, K.; Polit, W.; Winter, R. F.; Rheingold, A. L.; Novak, I. *Dalton Trans.* **2012**, *41*, 3675.
(12) Janiak, C.; Kuhn, N. *Adv. Nitrogen Heterocycl.* **1996**, *2*, 179.
(13) Kuhn, N.; Kuhn, A.; Lampe, E. M. *Chem. Ber.* **1991**, *124*, 997.
(14) Kuhn, N.; Jendral, K.; Boese, R.; Bläser, D. *Chem. Ber.* **1991**, *124*, 89.
(15) (a) Kuhn, N.; Köckerling, M.; Stubenrauch, S.; Bläser, D.; Boese, R. *J. Chem. Soc., Chem. Commun.* **1991**, 1368. (b) Kuhn, N.; Stubenrauch, S.; Boese, R.; Bläser, D. *J. Organomet. Chem.* **1992**, *440*, 289. (c) Kuhn, N.; Henkel, G.; Kreutzberg, J.; Stubenrauch, S.; Janiak, C. *J. Organomet. Chem.* **1993**, *456*, 97. (d) Kuhn, N.; Jendral, K.; Stubenrauch, S.; Mynott, R. *Inorg. Chim. Acta* **1993**, *206*, 1. (e) Licciulli, S.; Albahily, K.; Fomitcheva, V.; Korobkov, I.; Gambarotta, S.; Duchateau, R. *Angew. Chem., Int. Ed.* **2011**, *50*, 2346.
(16) (a) Schumann, H.; Winterfeld, J.; Hemling, H.; Kuhn, N. *Chem. Ber.* **1993**, *126*, 2657. (b) Schumann, H.; Rosenthal, E. C. E.; Winterfeld, J.; Kociok-Koehn, G. *J. Organomet. Chem.* **1995**, *495*, C12. (c) Schumann, H.; Rosenthal, E. C. E.; Winterfeld, J.; Weimann, R.; Demtschuk, J. *J. Organomet. Chem.* **1996**, *507*, 287. (d) Nishiura, M.; Mashiko, T.; Hou, Z. *Chem. Commun.* **2008**, 2019.
(17) (a) Schumann, H.; Gottfriedsen, J.; Demtschuk, J. *Chem. Commun.* **1999**, 2321. (b) Schumann, H.; Gottfriedsen, J.; Demtschuk, J. *Chem. Commun.* **1999**, 2091. (c) Kuhn, N.; Henkel, G.; Stubenrauch, S. *J. Chem. Soc., Chem. Commun.* **1992**, 760. (d) Kuhn, N.; Henkel, G.; Stubenrauch, S. *Angew. Chem., Int. Ed. Engl.* **1992**, *31*, 778. (e) Westerhausen, M.; Wieneke, M.; Noeth, H.; Seifert, T.; Pfitzner, A.; Schwarz, W.; Schwarz, O.; Weidlein, J. *Eur. J. Inorg. Chem.* **1998**, 1175.
(18) The trivial name trozircene is derived from tropylium.
(19) Kreye, M.; Gloeckner, A.; Daniliuc, C. G.; Freytag, M.; Jones, P. G.; Tamm, M.; Walter, M. D. *Dalton Trans.* **2013**, *42*, 2192.
(20) (a) Glöckner, A.; Arif, A. M.; Ernst, R. D.; Bannenberg, T.; Daniliuc, C. G.; Jones, P. G.; Tamm, M. *Inorg. Chim. Acta* **2010**, *364*, 23. (b) Glöckner, A.; Bannenberg, T.; Büschel, S.; Daniliuc, C. G.; Jones, P. G.; Tamm, M. *Chem. Eur. J.* **2011**, *17*, 6118. (c) Glöckner, A.; Bannenberg, T.; Tamm, M.; Arif, A. M.; Ernst, R. D. *Organometallics* **2009**, *28*, 5866. (d) Glöckner, A.; Bauer, H.; Maekawa, M.; Bannenberg, T.; Daniliuc, C. G.; Jones, P. G.; Sun, Y.; Sitzmann, H.; Tamm, M.; Walter, M. D. *Dalton Trans.* **2012**, *41*, 6614. (e) Glöckner, A.; Daniliuc, C. G.; Freytag, M.; Jones, P. G.; Tamm, M. *Chem. Commun.* **2012**, *48*, 6598. (f) Glöckner, A.; Tamm, M.; Arif, A. M.; Ernst, R. D. *Organometallics* **2009**, *28*, 7041. (g) Glöckner, A.; Bannenberg, T.; Daniliuc, C. G.; Jones, P. G.; Tamm, M. *Inorg. Chem.* **2012**, *51*, 4368. (h) Glöckner, A.; Kronig, S.; Bannenberg, T.; Daniliuc, C. G.; Jones, P. G.; Tamm, M. *J. Organomet. Chem.* **2013**, *723*, 181. (i) Glöckner, A.; Tamm, M. *Chem. Soc. Rev.* **2013**, *42*, 128.
(21) Maekawa, M.; Roemelt, M.; Daniliuc, C. G.; Jones, P. G.; White, P. S.; Neese, F.; Walter, M. D. *Chem. Sci.* **2012**, *3*, 2972.
(22) (a) Sitzmann, H.; Dezember, T.; Kaim, W.; Baumann, F.; Stalke, D.; Kärcher, J.; Dormann, E.; Winter, H.; Wachter, C.; Kelemen, M. *Angew. Chem., Int. Ed. Engl.* **1996**, *35*, 2872. (b) Wallasch, M.; Wolmershäuser, G.; Sitzmann, H. *Angew. Chem., Int. Ed.* **2005**, *44*, 2597. (c) Wallasch, M. W.; Rudolphi, F.; Wolmershäuser, G.; Sitzmann, H. *Z. Naturforsch., B* **2009**, *64*, 11. (d) Wallasch, M. W.; Vollmer, G. Y.; Kafiyatullina, A.; Wolmershäuser, G.; Jones, P. G.; Mang, M.; Meyer, W.; Sitzmann, H. *Z. Naturforsch., B* **2009**, *64*, 18. (e) Wallasch, M. W.; Weismann, D.; Riehn, C.; Ambrus, S.; Wolmershäuser, G.; Lagutschenkov, A.; Niedner-Schatteburg, G.; Sitzmann, H. *Organometallics* **2010**, *29*, 806. (f) Weismann, D.; Sun, Y.; Lan, Y.; Wolmershäuser, G.; Powell, A. K.; Sitzmann, H. *Chem. Eur. J.* **2011**, *17*, 4700. (g) Walter, M. D.; White, P. S. *New J. Chem.* **2011**, *35*, 1842. (h) Walter, M. D.; Grunenberg, J.; White, P. S. *Chem. Sci.* **2011**, *2*, 2120. (i) Walter, M. D.; White, P. S. *Inorg. Chem.* **2012**, *51*, 11860. (j) Walter, M. D.; White, P. S. *Dalton Trans.* **2012**, *41*, 8506.
(23) Kreye, M. Master's Thesis, TU Braunschweig, 2011.
(24) Anet, F. A. L.; Bourn, A. J. R. *J. Am. Chem. Soc.* **1967**, *89*, 760.
(25) Kuhn, N.; Horn, E. M.; Boese, R.; Blaeser, D. *Chem. Ber.* **1989**, *122*, 2275.
(26) (a) Lemoine, P.; Gross, M.; Braunstein, P.; Mathey, F.; Deschamps, B.; Nelson, J. H. *Organometallics* **1984**, *3*, 1303. (b) Audebert, P.; Miomandre, F.; Zakrzewski, J. *J. Electroanal. Chem.* **2002**, *530*, 63. (c) Kowalski, K.; Winter, R. F. *J. Organomet. Chem.* **2009**, *694*, 1041.
(27) Nakashima, S.; Kitao, T.; Matsunaga, H.; Kimura, I.; Inamura, H.; Okuda, T.; Sakai, H. *J. Radioanal. Nucl. Chem.* **1999**, *239*, 279.
(28) Burkey, D. J.; Hays, M. L.; Duderstadt, R. E.; Hanusa, T. P. *Organometallics* **1997**, *16*, 1465.
(29) Janiak, C.; Scharmann, T. G.; Green, J. C.; Parkin, R. P. G.; Kolm, M. J.; Riedel, E.; Mickler, W.; Elguero, J.; Charamunt, R. M.; Sanz, D. *Chem. Eur. J.* **1996**, *2*, 992.
(30) (a) Lemoine, P.; Gross, M.; Braunstein, P.; Mathey, F.; Deschamps, B.; Nelson, J. H. *J. Organomet. Chem.* **1985**, *295*, 189. (b) Lemoine, P. *J. Organomet. Chem.* **1989**, *359*, 61.
(31) (a) Gossauer, A. *Die Chemie der Pyrrole*; Springer-Verlag: Berlin, 1974. (b) Libert, M.; Caullet, C. *Bull. Soc. Chim. Fr.* **1971**, 1947. (c) Libert, M.; Caullet, C.; Longchamp, M. S. *Bull. Soc. Chim. Fr.* **1971**, 2367. (d) Andrieux, C. P.; Hapiot, P.; Audebert, P.; Guyard, L.; Dinh, An, M. N.; Groenendaal, L.; Meijer, E. W. *Chem. Mater.* **1997**, *9*, 723.
(32) Connelly, N. G.; Geiger, W. E. *Chem. Rev.* **1996**, *96*, 877.
(33) Okuda, J.; Albach, R. W.; Herdtweck, E.; Wagner, F. E. *Polyhedron* **1991**, *10*, 1741.
(34) Maekawa, M.; Daniliuc, C. G.; Freytag, M.; Jones, P. G.; Walter, M. D. *Dalton Trans.* **2012**, *41*, 10317.

(35) (a) Zahn, U.; Kienle, P.; Eicher, H. *Z. Phys.* **1962**, *166*, 220. (b) Wertheim, G. K.; Herber, R. H. *J. Chem. Phys.* **1963**, *38*, 2106.
(36) Roberts, R. M. G.; Silver, J.; Ranson, R. J.; Morrison, I. E. G. *J. Organomet. Chem.* **1981**, *219*, 233.
(37) (a) Greenwood, N. N.; Gibb, T. C. In *Mössbauer Spectroscopy*; Chapman and Hall: London, 1971, p 233. (b) Collins, R. L. *J. Chem. Phys.* **1965**, *42*, 1072.
(38) Ernst, R. D.; Wilson, D. R.; Herber, R. H. *J. Am. Chem. Soc.* **1984**, *106*, 1646.
(39) Houlton, A.; Roberts, R. M. G.; Silver, J.; Zakrzewski, J. *J. Organomet. Chem.* **1993**, *456*, 107.
(40) Guimon, C.; Gonbeau, D.; Pfister-Guillouzo, G.; de Lauzon, G.; Mathey, F. *Chem. Phys. Lett.* **1984**, *104*, 560.
(41) (a) Birchall, T.; Drummond, I. *Inorg. Chem.* **1971**, *1971*, 399. (b) Herber, R. H.; Hanusa, T. P. *Hyperfine Interact.* **1997**, *108*, 563. (c) Abraham, M.; Klauß, H. H.; Wagener, W.; Litterst, F. J.; Hofmann, A.; Herberhold, M. *Hyperfine Interact.* **1999**, *120−121*, 253.
(42) Stukan, R. A.; Gubin, S. P.; Nesmeyanov, A. N.; Gol'danskii, V. I.; Makarov, E. F. *Teor. Eksp. Khim.* **1966**, *2*, 805.
(43) Houlton, A.; Miller, J. R.; Roberts, R. M. G.; Silver, J. *J. Chem. Soc., Dalton Trans.* **1991**, *0*, 467.
(44) Roberts, R. M. G.; Silver, J.; Wells, A. S. *Inorg. Chim. Acta* **1986**, *119*, 1.
(45) Blume, M.; Tjon, J. A. *Phys. Rev.* **1968**, *165*, 446.
(46) Prins, P. *Mol. Phys.* **1970**, *19*, 603.
(47) Cramer, C. J.; Truhlar, D. G. *Phys. Chem. Chem. Phys.* **2009**, *11*, 10757.
(48) Grimme, S. *J. Comput. Chem.* **2006**, *27*, 1787.
(49) (a) Brandhorst, K.; Grunenberg, J. *Chem. Soc. Rev.* **2008**, *37*, 1558. (b) Grunenberg, J. *Phys. Chem. Chem. Phys.* **2011**, *13*, 10136.
(50) Stoll, S.; Schweiger, A. *J. Magn. Reson.* **2006**, *178*, 42.
(51) (a) Sheldrick, G. M. In *SHELXL-97, Program for the Refinement of Crystal Structure from Diffraction Data*; University of Göttingen, Göttingen, Germany, 1997. (b) Sheldrick, G. M. *Acta Crystallogr.* **2008**, *A64*, 112.
(52) Job, R.; Earl, R. *Inorg. Nucl. Chem. Lett.* **1979**, *15*, 81.
(53) Heyn, B.; Hipler, B.; Kreisel, G.; Schreer, H.; Walther, D. *Anorganische Synthesechemie - Ein integriertes Praktikum*; Springer-Verlag: Berlin, 1986.
(54) Frisch, M. J.; Trucks, G. W.; Schlegel, H. B.; Scuseria, G. E.; Robb, M. A.; Cheeseman, J. R.; Scalmani, G.; Barone, V.; Mennucci, B.; Petersson, G. A.; Nakatsuji, H.; Caricato, M.; Li, X.; Hratchian, H. P.; Izmaylov, A. F.; Bloino, J.; Zheng, G.; Sonnenberg, J. L.; Hada, M.; Ehara, M.; Toyota, K.; Fukuda, R.; Hasegawa, J.; Ishida, M.; Nakajima, T.; Honda, Y.; Kitao, O.; Nakai, H.; Vreven, T.; Montgomery, J. A., Jr.; Peralta, J. E.; Ogliaro, F.; Bearpark, M.; Heyd, J. J.; Brothers, E.; Kudin, K. N.; Staroverov, V. N.; Kobayashi, R.; Normand, J.; Raghavachari, E.; Rendell, A.; Burant, J. C.; Iyengar, S. S.; Tomasi, J.; Cossi, M.; Rega, N.; Millam, J. M.; Klene, M.; Knox, J. E.; Cross, J. B.; Bakken, V.; Adamo, C.; Jaramillo, J.; Gomperts, R.; Stratmann, R. E.; Yazyev, O.; Austin, A. J.; Cammi, R.; Pomelli, C.; Ochterski, J. W.; Martin, R. L.; Morokuma, K.; Zakrzewski, V. G.; Voth, G. A.; Salvador, P.; Dannenberg, J. J.; Dapprich, S.; Daniels, A. D.; Farkas, O.; Foresman, J. B.; Ortiz, J. V.; Cioslowski, J.; Fox, D. J. In *Gaussian 09, Revision A.02*; Gaussian, Inc., Wallingford, CT, 2009.